Journal of Materials Chemistry A

ROYAL SOCIETY OF CHEMISTRY

PAPER

View Article Online
View Journal | View Issue

Cite this: J. Mater. Chem. A, 2025, 13, 34306

Atomic-scale insights into air electrode degradation after 10 years of fuel cell stack operation

Moritz Kindelmann, †*[ab] Olivier Guillon, [bc] Joachim Mayer[ad] and Norbert H. Menzler [b]

Solid oxide cells (SOCs) represent a key technology for sustainable energy conversion due to their high efficiency and the ability to integrate them into energy intensive industrial processes. Designing solid oxide stack systems that exhibit long-term durability is challenging, due to the harsh operating conditions for all applied materials, particularly at the air electrode side. In this study, we investigate the degradation mechanisms at the $La_{0.58}Sr_{0.4}Co_{0.2}Fe_{0.8}O_{3-\delta}$ (LSCF) air electrode of a solid oxide fuel cell (SOFC) short stack, which was operated for 93 000 hours in fuel cell mode at 700 °C under a constant current density of 0.5 A cm^{-2}, with 40% fuel utilization and hydrogen and oxygen as feed gases. We apply atomic-resolution scanning transmission electron microscopy and spectroscopy to analyze changes in structure and chemistry across the electrode and its interface with the Gd-doped ceria (GDC) diffusion barrier. While the bulk of the LSCF electrode mostly retained structural integrity with only minor local changes, significant degradation occurred at the LSCF–GDC interface. Heavy Sr leaching induced by chromium poisoning led to the formation of micron-sized $SrCrO_4$ crystallites. Simultaneously, Cr-containing decomposition products reacted with GDC to form substituted CeO_2-based nanoparticles, triggering gradual delamination of the electrode. These nanoscale interactions disrupted the contact between the air electrode and barrier, significantly contributing to cell failure. Our findings provide critical insights into long-term degradation in SOCs and emphasize the need for improved material combinations to ensure stable operation over extended lifetimes.

Received 15th May 2025
Accepted 27th August 2025

DOI: 10.1039/d5ta03917g

rsc.li/materials-a

Introduction

The transition to sustainable energy systems necessitates the development of novel energy conversion devices that rely on CO_2-free resources. Among these, solid oxide cells (SOCs) are particularly promising due to their high energy conversion efficiencies at elevated temperatures and their potential for integration into energy-intensive industrial processes as both fuel cells and electrolysis systems.[1,2] Under the harsh operational environments of SOCs – characterized by temperatures between 600 and 900 °C, constant electrical bias, and exposure to corrosive atmospheres – all applied materials in the stack system must withstand a multitude of degradation mechanisms to enable long term applicability of the system.[3]

The degradation of air electrodes and the associated loss of conversion efficiency is a critical challenge for SOC stack performance and longevity. Materials for air electrodes applied in SOCs are mostly based on ferrite (*e.g.* $La_{0.6}Sr_{0.4}Co_{0.2}Fe_{0.8}O_{3-\delta}$, LSCF), cobaltite ($La_{0.6}Sr_{0.4}Co_{3-\delta}$, LSC) or manganite (*e.g.* $La_{0.65}Sr_{0.3}O_{3-\delta}$, LSM) perovskite ceramics, all of which are composed of a mixture of La and Sr on the A-site.[4,5] Due to increased performance compared to LSM, state of the art cell concepts mostly use electrodes using different LSC(F) perovskites.[2] Under application conditions, LSC(F) electrodes show two primary mechanisms of degradation: Firstly, Sr segregation to the surface: this effect occurs after short-term application and is caused by cation size mismatch and charge interaction[6–9] leading to deteriorated surface chemistry and a decrease in oxygen exchange kinetics.[9] Secondly, Cr poisoning of the LSC(F) electrode: this mechanism emerges during prolonged operation under full stack conditions, due to the evaporation of Cr-rich species from corrosion resistant steel interconnects.[10,11] Chromium poisoning leads to a multitude of effects, including phase decomposition[12,13] and surface chemistry changes,[14–17] which after prolonged exposure lead to a decrease in the electrode

[a]Forschungszentrum Jülich GmbH, Ernst Ruska-Centre for Microscopy and Spectroscopy with Electrons (ER-C), 52425 Jülich, Germany. E-mail: mokin@dtu.dk
[b]Forschungszentrum Jülich GmbH, Institute of Energy Materials and Devices, Materials Synthesis and Processing (IMD-2), 52425, Jülich, Germany. E-mail: n.h.menzler@fz-juelich.de
[c]Jülich Aachen Research Alliance, JARA-Energy, 52425, Jülich, Germany
[d]RWTH Aachen University, Central Facility for Electron Microscopy (GFE), 52074 Aachen, Germany
† Now at Technical University of Denmark, Department of Energy Conversion and Storage (DTU Energy), 2800 Kongens Lyngby, Denmark.

performance.[18,19] Both mechanisms strongly compromise electrode functionality and significantly impact device durability.

A broad body of work is available that has theoretically investigated the thermodynamics[12,20–23] and experimentally validated the kinetics of the Cr-poisoning reaction with lanthanum ferrites and manganites.[11,13,15–17,19,24] In particular, ferrites containing less stable tetravalent cations (Fe^{3+} and Co^{3+}) tend to form $SrCrO_4$ as a reaction product during degradation in contact with volatile CrO_3 species that form from ferritic steels in application environments.

Due to the substantial economic and temporal investments required for long-term testing under real-world stack conditions, most studies focus on short-term investigations or utilize simplified model architectures to assess the degradation mechanisms.[12,25–27] These efforts have helped to understand the basic mechanisms that govern microstructure and phase changes under CrO_x exposure and constant polarization, leading to the formation of $SrCrO_4$ at the contact layer as well as inside the porous air electrode.[28,29] In contrast, only a limited number of publications explore the effects of long-term testing (>20 000 h) under realistic stack conditions, with Forschungszentrum Jülich conducting some of the most notable studies in this area.[18,19,30–32]

Among them, a short stack consisting of two anode-supported cells (ASCs) was tested for an unprecedented 93 000 h in fuel cell mode under a constant current density of 0.5 A cm^{-2}, with 40% fuel utilization and hydrogen and oxygen as feed gases. This represents the longest SOFC stack test conducted to date and the first detailed investigation into the end-of-life performance and failure mechanisms of high-temperature oxide fuel cells.[32] Here, we utilize atomic-resolution scanning transmission electron microscopy to study the nanoscale degradation and failure mechanisms at the air electrode side after long-term operation under real application environments.

Alongside the oxidation of metallic components, the degradation of the SOC stack was driven by the disintegration of the interface between the Gd-doped ceria (GDC) diffusion barrier and the $La_{0.58}Sr_{0.4}Co_{0.2}Fe_{0.8}O_{3-\delta}$ (LSCF) electrode. This failure mechanism is activated by the specific local oxygen partial pressure, which facilitates the deposition of evaporated Cr species and the subsequent formation of secondary phases directly at the GDC interface.[12,32,33] The Cr deposition led to severe Sr leaching from the LSCF, resulting in the formation of micrometer-sized $SrCrO_4$ crystals decorating the interface. This phenomenon has been observed previously at lower resolution but could not be completely resolved.[32,33] Concurrently, the GDC diffusion barrier reacted with the decomposition products of Cr-poisoned LSCF, forming highly substituted CeO_2 solid solution nanoparticles. This overlooked interaction caused progressive damage to the interface, reducing the contact area between the electrode and the oxygen ion-conducting electrolyte. The continuing loss of contact area contributed to the continuous performance loss during operation, ultimately leading to cell failure at the end of life.

This study provides novel high resolution insights into the nanoscale mechanisms that drive long-term degradation in SOFCs, highlighting the importance of developing materials, protection layers and material combinations that are capable of withstanding the challenging environments during prolonged operation.

Results and discussion

Stability of LSCF air electrodes

Fig. 1 provides an overview of the cell design used in this study (a), a schematic graph of the performance loss during operation (b), the microstructure of the cell (c) and the GDC–LSCF interface after long-term operation (d and e). Both cells tested in the short stack show a non-linear degradation behavior, separated into three zones: zones I and II describe the slightly non-linear performance degradation with a voltage drop of 1%/kh during the first 40 000 h, which is assumed to be connected to the corrosion of interconnects and Cr poisoning of the air electrode.

Afterwards, the degradation rate in zone III dropped drastically to around 0.1%/kh and remained stable until the end of life. Connecting the global degradation behavior to microstructural features at the end of life of an SOFC system is challenging, therefore we focus on the complex changes that occur at the interface between the LSCF electrode and GDC diffusion barrier. The STEM image and the EDS mapping in Fig. 1d and e highlight several important degradation features, which have led to cell degradation and failure: (1) large grains of a Sr- and Cr-rich secondary oxide phase, (2) nanoscale particle formation directly at the interface. Both of these features can be observed using SEM based techniques and have been reported previously using low magnification techniques.[12,32,33] The structure, chemistry and possible formation mechanisms will be discussed in detail in the following paragraphs.

Firstly, we investigated the stability of the LSCF electrode at positions with different distances from the GDC interface. Therefore, two positions were selected: (I) close to the GDC interface but not in contact (roughly 500 nm from the interface), (II) away from the interface (approximately 7 μm from the interface). Both positions are of interest, as during fuel cell operation the oxygen and chromium partial pressures differ across the thickness of the air electrode,[12] opening the possibility for different electrode material stabilities. The stability of LSCF during long-term electrochemical application has been under discussion since its introduction as an air electrode in SOC cell assemblies. Especially, Sr surface segregation can be detrimental for the oxygen exchange reaction (OER) performance of LSCF. Therefore, high resolution imaging and spectroscopy were used to investigate the integrity of LSCF at both selected positions. Fig. 2 shows an overview image of the porous electrode structure (a) and high resolution high-angle annular dark field (HAADF) images of the atomic structure in the bulk (b) and at the surface of LSCF (c), roughly 500 nm from the GDC interface. The LSCF particle in Fig. 2(a) is aligned down the [111] direction of the cubic perovskite crystal, enabling atomic resolution imaging, which makes it possible to assess crystallographic defects or phase changes. Despite the long-term exposure to application conditions, both images highlight the pristine nature of the perovskite phase, which shows that no crystalline defects or secondary phases have formed after long-term application.

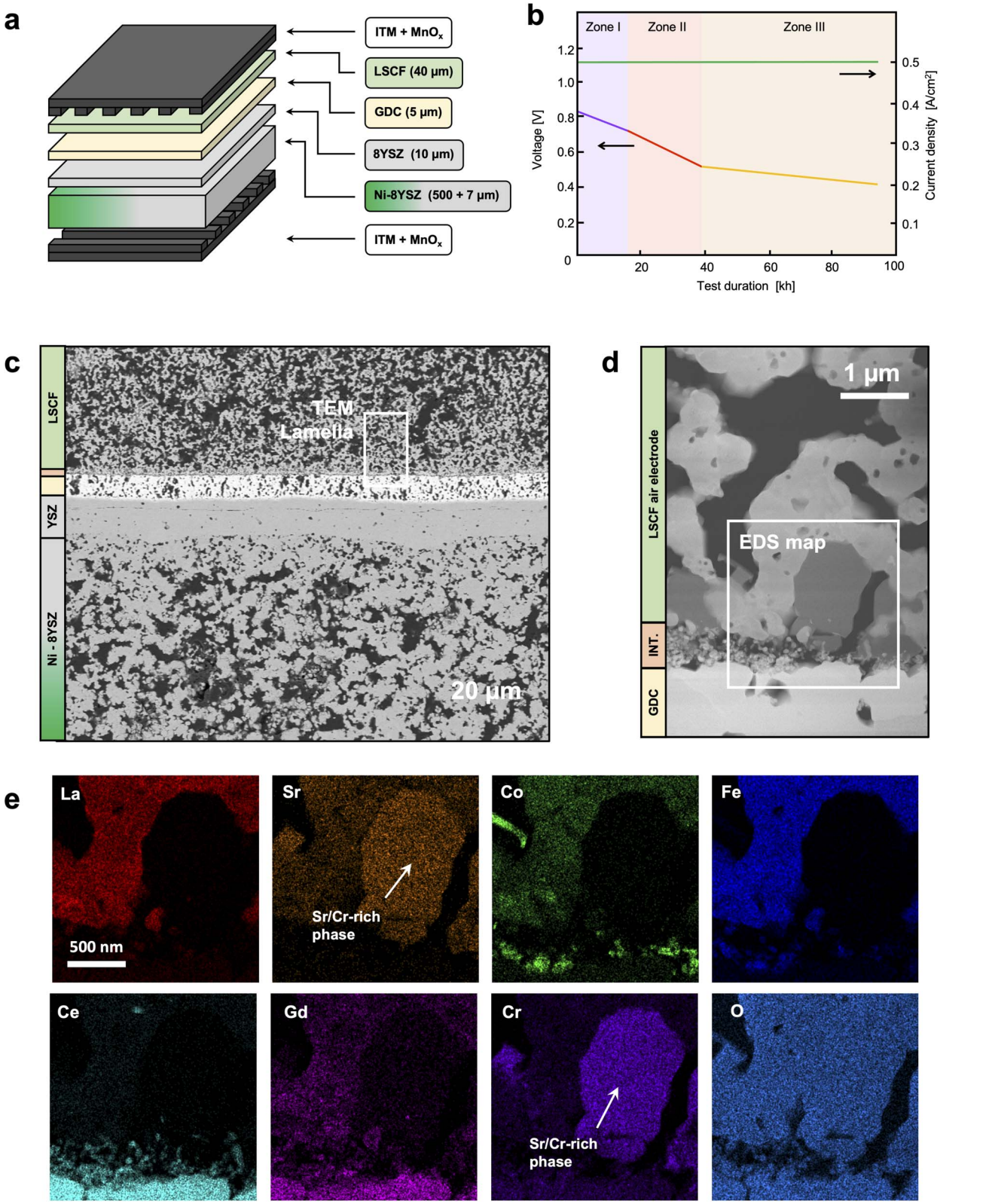

Fig. 1 Overview of the LSCF microstructure after 100 000 hours of fuel cell operation. (a) Schematic representation of the anode supported fuel cell architecture. (b) Schematic graph showing the performance of the SOFC short stack over 93 000 h. Details on the electrochemical performance can be found elsewhere.[30] (c) Overview SEM image of the cross section of the full cell after operation. (d) HAADF STEM overview image of the interface between the GDC diffusion barrier and the LSCF air electrode. (e) Overview EDS mapping of the degraded GDC–LSCF interface. The corresponding area is highlighted in (d). In the following the focus is on the LSCF air electrode and its interface to the GDC diffusion barrier.

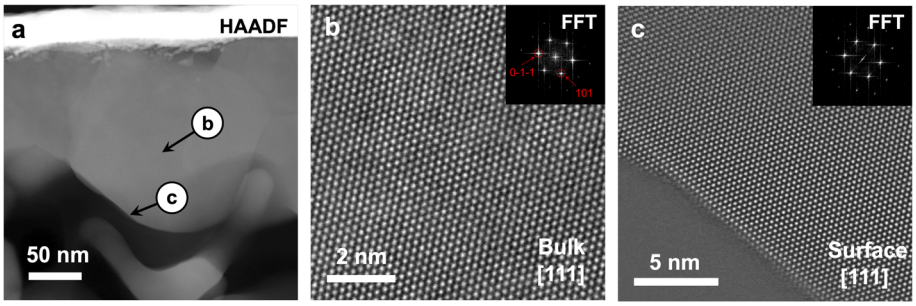

Fig. 2 High resolution structural imaging of LSCF located close to the interface (500 nm). (a) Overview HAADF image of a LSCF grain oriented along the [111] direction. The bright feature at the top of the image is a Pt protection layer that was applied for sample preparation reasons. (b) and (c) High resolution HAADF images of the atomic structure of LSCF in the bulk and at the surface of the particle imaged in (a). The locations where the images were taken are highlighted in (a).

Comparable observations could be made for LSCF located several microns (*ca.* 7 μm) away from the GDC interface. Fig. 3 provides an overview image (a) as well as atomic resolution images and elemental spectroscopy (b and c) from one LSCF grain. For high resolution imaging, the grain is oriented along the [110] direction. This crystallographic orientation allows to image the *A*- and *B*-plane separately, making high resolution energy dispersive X-ray spectroscopy (EDS) mapping of the atomic structure possible (c). Even though locations further away from the GDC interface display a different local pO_2 and $p(CrO_3)$ environment,[12] these changes do not seem to strongly influence the stability of LSCF. Both the bulk and surface of the investigated perovskite grain show a pristine perovskite crystal structure (Fig. 3b and c). A fast Fourier transform (FFT) analysis of both high resolution images confirms the cubic crystal structure of LSCF ($Pm\bar{3}m$, Nr. 221, ICSD 246266). High resolution EDS mapping of the atomic structure of

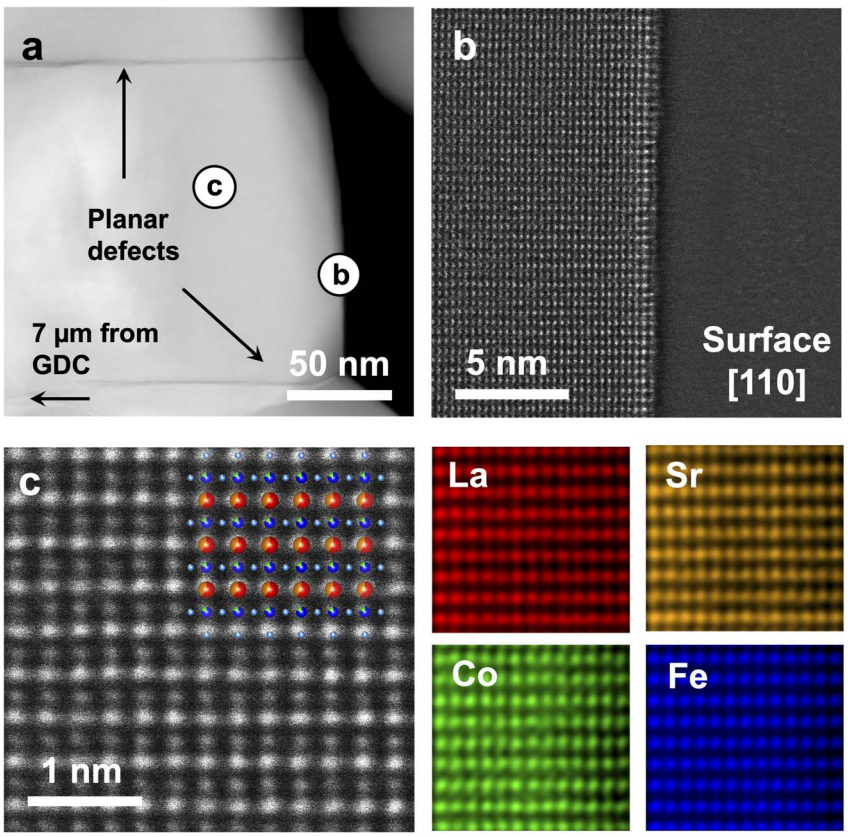

Fig. 3 High resolution structural and spectroscopic imaging of LSCF far from the interface. (a) Overview HAADF image of a LSCF grain 7 μm away from the interface. The overview image shows planar defects (additional high-resolution images in Fig. 4) and a slight contrast change central in the grain, which can be associated with Co-rich secondary phases (additional EDS mapping in Fig. 4). (b) and (c) High resolution HAADF images of LSCF oriented along the [110] direction showing the atomic structure in the bulk and at the surface. (c) Atomic resolution EDS mapping at the bulk position. An overlay shows a model of the crystal structure of LSCF ($La_{0.6}Sr_{0.4}Co_{0.2}Fe_{0.8}O_3$).

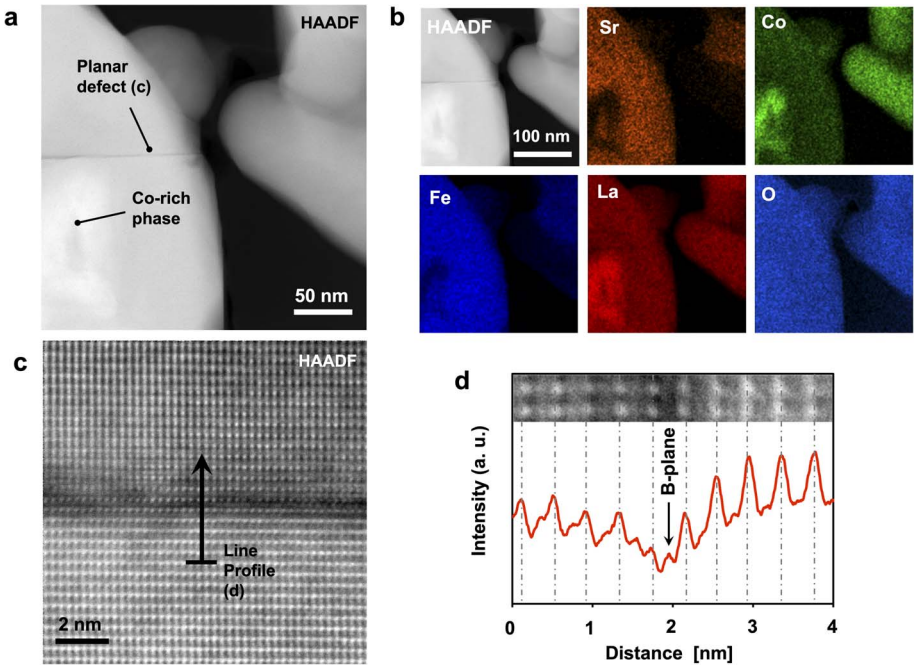

Fig. 4 High resolution structural and spectroscopic imaging of LSCF far from the interface. (a) Overview HAADF image of a LSCF grain 7 μm away from the interface. (b) EDS mapping of the image shown in (a). (c) Atomic resolution HAADF image of a Non-Ruddlesden–Popper (NPR) type stacking fault. (d) Intensity profile across the stacking fault showing the strong B-site depletion on one atomic plane.

LSCF additionally highlights the stability of the majority of the electrode material (excluding planar defects) after long-term application until the end of life.

The local variations visible in the HAADF image (Fig. 3a) can be associated with planar defects that formed due to inhomogeneities in perovskite stoichiometry and Co-rich secondary

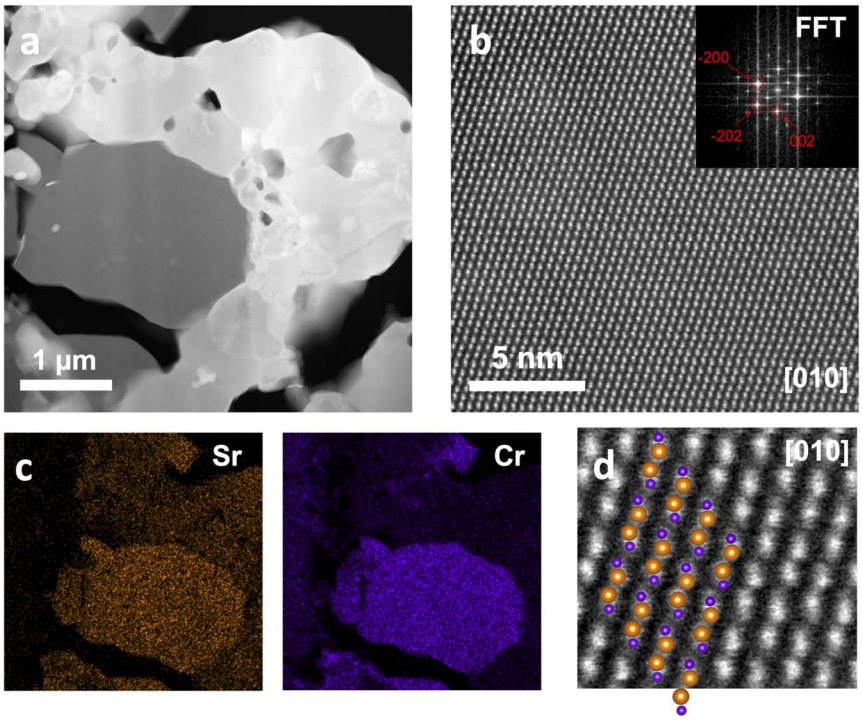

Fig. 5 Structure and chemistry of the strontium chromate phase at the LSCF–GDC interface. (a) Overview HAADF image showing a large secondary particle that is embedded in the porous LSCF microstructure at the interface. (b) Atomic resolution HAADF image of the $SrCrO_4$ grain in (a). An FFT of the image is embedded in the top. (c) EDS mapping of the overview area revealing a large amount of Cr-poisoning. (d) Overlay of the crystallographic structure ($SrCrO_4$, $P2_1/c$ Nr. 14, ICSD 160793) onto the atomic structure image. Orange and purple spheres represent Sr and Cr atoms.

phases. Fig. 4 gives additional details on the Co-rich secondary phases (b) and the atomic structure of planar defects (c and d). The EDS mapping helps to reveal the local chemistry of the La and Co-rich secondary phase, which is visible as a bright area inside the LSCF grain. Further Co-rich particles are visible on the right hand side of the investigated area. These secondary phases might be induced by the intended off-stoichiometry used in the starting material or due to Sr leaching triggered by Cr-poisoning. However, reference measurements of the microstructure of a pristine LSCF electrode in a similar cell architecture show similar Co-rich inclusions (SI Fig. S1 and S2), proving that these secondary phases have been present during the whole test, and seem to play a minor role during performance degradation of the SOFC stack.

Furthermore, high resolution imaging of the planar defect (Fig. 4c and d) reveals the atomic structure of these stacking fault type defects. A line profile of the image intensity across the atomically sharp defect shows that strong B-site depletion can be observed, fitting a similar observation that Jennings *et al.* have recently made in the perovskite-type proton conducting ceramic $BaZr_{0.8}Y_{0.2}O_{3-\delta}$ (BZY), when an off-stoichiometry in the *A*/*B* ratio is forcefully induced.[34] These observations show that long-term exposure to Cr poisoning under application conditions has led to stoichiometry changes in the LSCF electrode, which are compensated for by the formation of stacking faults (which could not be observed in reference electrodes). However, what influence these very local structural changes have on the overall performance of the LSCF electrode is not clear. A significantly higher density of stacking faults in BZY had only a minor impact on the bulk electrochemical performance,[34] implying a similar behavior in LSCF.

Despite the long-term application of the LSCF electrode under load at 700 °C, only minor microstructural and local crystallographic changes in the bulk and at the surface could be

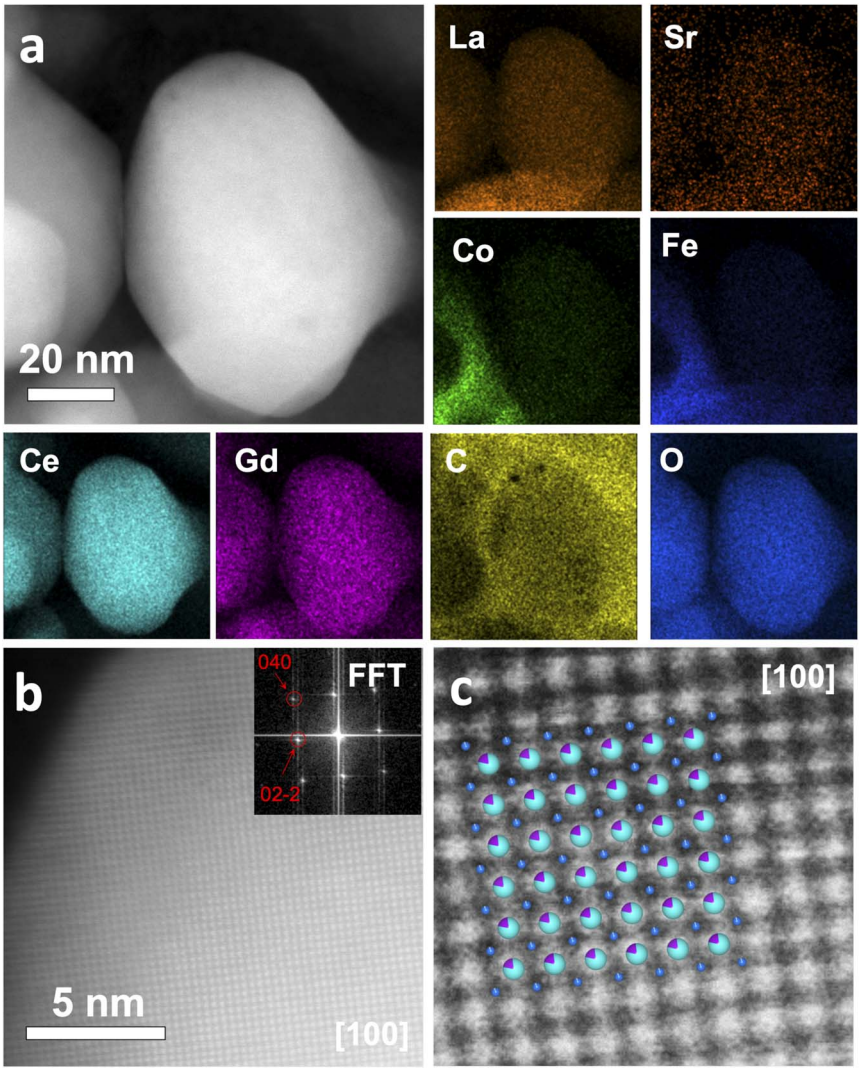

Fig. 6 Structure and chemistry of the decomposition phase at the GDC side of the LSCF–GDC interface. (a) HAADF image and corresponding EDS mapping of a nanoparticle that formed after long-term testing. (b) High resolution image of the particle along the [100] direction. A FTT of the image is embedded in the top right. (c) Overlay of the crystallographic structure ($Ce_{0.8}Gd_{0.2}O_{1.8}$, $Fm\bar{3}m$ Nr. 225, ICSD 182976) onto the atomic structure image. Blue, turquoise and purple spheres represent O, Ce and Gd atoms, respectively.

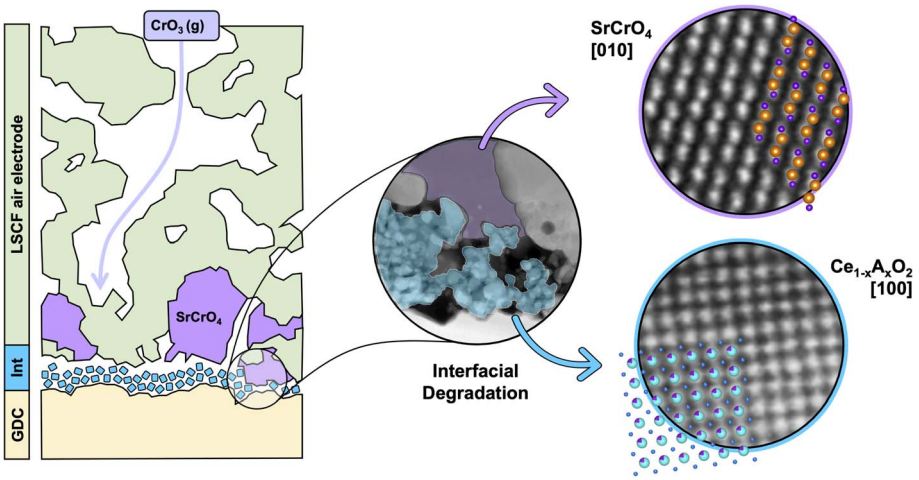

Fig. 7 Summary of the nanoscale degradation mechanism of the LSCF–GDC interface after long-term fuel cell operation. The deposition of CrO_3 at the interface leads to a strong decomposition of LSCF through Sr leaching and the formation of $SrCrO_4$. Residuals of this decomposition interact with the diffusion barrier and form highly substituted $Ce_{1-x}A_xO_2$ nanoparticles that lead to a continuous delamination of the air electrode.

observed. At both investigated positions, the perovskite crystal structure was mostly intact, and we expect that only a small portion of the performance degradation can be attributed to the disintegration in the bulk of the electrode, and most of the damage was induced at the LSCF–GDC interface.

Degradation of the LSCF–GDC interface

The interface between the LSCF air electrode and the GDC diffusion barrier is of specific interest due to the deposition of large amounts of $SrCrO_4$ and the associated deterioration that was observed after stack testing.[12,32,35] Therefore, we investigated the phases present at the interface in detail to derive a deeper understanding of the degradation at the interface. Fig. 5 provides an overview of the microstructure and the atomic structure of the Sr and Cr-rich phase that has formed predominantly close to the GDC layer.

In the investigated areas, several large, micron-sized Sr and Cr-rich particles formed (Fig. 5a and c, additional imaging and EDS mapping from the degraded LSCF–GDC interface are presented in SI Fig. S3 and S4), highlighting the severity of Sr leaching from LSCF. Atomic resolution imaging (Fig. 5b) of the large crystallite in Fig. 5a enables the determination of the crystal structure of the secondary phase ($SrCrO_4$, $P2_1/c$ Nr. 14, ICSD 160793). The included FFT in Fig. 5b matches the crystal structure when compared to a theoretical diffraction pattern. To further visualize this, a model of the crystal structure is overlaid onto the HAADF image in Fig. 5d. Contrary to thermodynamic calculations which predicted the formation of other stoichiometries of the strontium chromite phase ($SrCrO_3$),[12] we now only observed the monoclinic $SrCrO_4$ phase, which is also regularly reported as a decomposition product.

The predominant formation of the $SrCrO_4$ at the interface furthermore induces secondary phase nanoparticles that decorate the interface and lead to a continuous detachment of the air electrode. Fig. 6 summarizes the chemical composition and atomic structure of a representative nanoparticle that formed after long-term application. The EDS mapping reveals the complex composition of the nanoparticle, which consists primarily of Ce and Gd but also hosts residuals of the decomposed LSCF. A standardless quantification showed concentrations of roughly 7–8 at% La, 2–3 at% of Fe and 1.5 at% of Co in this specific nanoparticle (details can be found in SI Fig. S5). Adjacent to the investigated particle, Co and Fe-rich oxides can be found, which is proof of the high elemental heterogeneity at the interface after degradation. High resolution imaging along the [100] direction of the same particle in Fig. 6b and c shows that the crystal structure of GDC ($Ce_{0.8}Gd_{0.2}O_{1.8}$, $Fm\bar{3}m$ Nr. 225, ICSD 182976) is maintained despite the additional elemental substitution that happened during degradation. An analysis of the included FFT image additionally shows a good match with the described crystal structure.

The major problem which is induced by the formation of a reaction product between the GDC layer and the residual of the decomposition of the LSCF due to Cr-poisoning is the effective separation of the air electrode from the oxygen ion conducting electrolyte. This degradation mechanism is visualized schematically in Fig. 7. The continuous delamination process, which is described here, might be one of the major factors inducing performance losses alongside the oxidation process and degradation at the contact layer. This effect could be specifically active in the stable degradation zone III (Fig. 1b) and therefore be one of the major contributors to the failure of the SOC stack after long-term application.

Conclusions

In this study, we investigated the degradation mechanisms in the air electrode layer of a solid oxide fuel cell short stack, which was operated at Forschungszentrum Jülich under load for 93 000 hours under realistic fuel cell conditions. We used atomic

resolution transmission electron microscopy and spectroscopy to analyze the nanoscale degradation mechanisms of the LSCF air electrode, and specifically its interface with the GDC diffusion barrier. After nearly 100 000 hours of continuous operation, the LSCF air electrode exhibited surprising structural and chemical stability considering the long-term exposure to harsh operating conditions. Atomic-resolution imaging confirmed the durability of the perovskite structure, with only minor planar defects (stacking faults) and secondary phases forming, suggesting that bulk electrode decomposition plays a limited role in the long-term performance loss during application.

The primary degradation on the air side occurred at the LSCF–GDC interface. Chromium evaporation from steel interconnects led to severe Sr leaching from LSCF and the subsequent formation of large $SrCrO_4$ crystals especially at the interface, a process that has previously only been characterized at low spatial resolution. In addition to the formation of large $SrCrO_4$ crystals, the interaction between the GDC diffusion barrier and Cr-contaminated LSCF decomposition products resulted in the formation of an interlayer of highly substituted CeO_2-based nanoparticles. These new phases forming at the interface detached the air electrode from the electrolyte and disrupted the electrochemical integrity of the interface. The progressive accumulation of secondary phases and the chemical degradation of the GDC–LSCF interface led to the observed delamination between the air electrode and the electrolyte. This delamination process is likely a major contributor to the gradual performance loss observed in the later stages of stack operation (here called zone III, Fig. 1b). The presented findings highlight the importance of material compatibly and interface design, specifically in systems that undergo the degradation phenomenon during long-term application. Future stack designs must focus on applying improved, high-quality Cr evaporation barrier coatings (with high density for optimal Cr-retention) that provide both good electronic contact and minimize Cr-poisoning of the functional layers. Improved protection layers could be combined with air electrode materials that show an increased Cr-resistance to further minimize the degradation during fuel and electrolyser applications at temperatures above 600 °C.

Experimental methods

Stack processing and long-term testing

Samples for the post-test characterization were taken from a disassembled two-layer short stack built from anode supported cells (ASC). The cells had an active area of 80 cm^2, and consisted of a 10 μm thick 8YSZ electrolyte layer, an $La_{0.58}Sr_{0.4}Co_{0.2}Fe_{0.8}O_{3-\delta}$ (LSCF) air electrode and a screen-printed GDC diffusion barrier. The cells were glass-ceramic sealed into ITM (Plansee SE, Austria) interconnector plates, which were coated on the air side with a MnO_x protective coating against Cr-evaporation. The long-term stationary testing in fuel cell mode was conducted under a constant current density of 0.5 A cm^{-2} at a furnace temperature of 700 °C, with a fuel utilization of 40% using H_2 and 40% O_2 utilization with compressed air. Details of the processing of cells, stack assembly and detailed electrochemical characterization can be found elsewhere.[36–38]

Transmission electron microscopy characterization

Samples for scanning transmission electron microscopy (STEM) were prepared using scanning electron microscopy/focused ion beam preparation (SEM-FIB, FEI Helios NanoLab 460F1, USA). The samples were taken at the GDC–LSCF interface from a metallographically polished cross-section of the tested cell, and a reference cell using a focused Ga^+ ion beam, with a final polishing energy of 2 kV. High resolution STEM imaging and spectroscopy were conducted using a probe corrected Spectra 300 microscope (Thermo Fischer Scientific, USA) at 200 keV using a probe current of 200 pA. The microscope was equipped with a Super-X EDS detector and the data analysis of the EDS results was done using the Velox software (Thermo Fischer Scientific, USA).

Author contributions

M. K. designed the study, prepared all TEM samples, characterized the structure and chemistry using electron microscopy and wrote the original manuscript. N. H. M., O. G. and J. M. acquired funding, discussed the results and supported the writing and editing.

Conflicts of interest

The authors declare that they have no known competing financial interests or personal relationships that could have appeared to influence the work reported in this paper.

Data availability

Data for this article, including raw electron microscopy files and EDS mapping are available at the Open Science Framework at **https://osf.io/qxmzp/** under DOI: **https://doi.org/10.17605/OSF.IO/QXMZP**.

Supplementary information is available. See DOI: **https://doi.org/10.1039/d5ta03917g**.

Acknowledgements

M. K. acknowledges the support from Lidia Kibkalo (ER-C, Forschungszentrum Jülich) during FIB lamella preparation and funding for this work from the German Science Foundation (DFG) under grants MA 1280/69-1 and KI 2997/1-1.

References

1 A. Hauch, *et al.*, Recent advances in solid oxide cell technology for electrolysis, *Science*, 2020, 370.
2 S. E. Wolf, *et al.*, Solid oxide electrolysis cells – current material development and industrial application, *J. Mater. Chem. A*, 2023, **11**, 17977–18028, DOI: **10.1039/d3ta02161k**.
3 Y. Wang, W. Li, L. Ma, W. Li and X. Liu, Degradation of solid oxide electrolysis cells: phenomena, mechanisms, and

emerging mitigation strategies—a review, *J. Mater. Sci. Technol.*, 2020, **55**, 35–55, DOI: 10.1016/j.jmst.2019.07.026.
4 A. Petric, P. Huang and F. Tietz, Evaluation of La-Sr-Co-Fe-O perovskites for solid oxide fuel cells and gas separation membranes, *Solid State Ionics*, 2000, **135**, 719–725.
5 A. Mai, V. A. C. Haanappel, S. Uhlenbruck, F. Tietz and D. Stöver, Ferrite-based perovskites as cathode materials for anode-supported solid oxide fuel cells: part I. Variation of composition, *Solid State Ionics*, 2005, **176**, 1341–1350.
6 M. Finsterbusch, A. Lussier, J. A. Schaefer and Y. U. Idzerda, Electrochemically driven cation segregation in the mixed conductor $La_{0.6}Sr_{0.4}Co_{0.2}Fe_{0.8}O_{3-\delta}$, *Solid State Ionics*, 2012, **212**, 77–80.
7 W. Lee, J. W. Han, Y. Chen, Z. Cai and B. Yildiz, Cation size mismatch and charge interactions drive dopant segregation at the surfaces of manganite perovskites, *J. Am. Chem. Soc.*, 2013, **135**, 7909–7925.
8 D. Kim, R. Bliem, F. Hess, J. J. Gallet and B. Yildiz, Electrochemical Polarization Dependence of the Elastic and Electrostatic Driving Forces to Aliovalent Dopant Segregation on $LaMnO_3$, *J. Am. Chem. Soc.*, 2020, **142**, 3548–3563.
9 Đ. Tripković, *et al.*, Thermally Controlled Activation and Passivation of Surface Chemistry and Oxygen-Exchange Kinetics on a Perovskite Oxide, *Chem. Mater.*, 2022, **34**, 1722–1736.
10 L. Zhou, J. H. Mason, W. Li and X. Liu, Comprehensive review of chromium deposition and poisoning of solid oxide fuel cells (SOFCs) cathode materials, *Renewable Sustainable Energy Rev.*, 2020, **134**, 110320.
11 R. Wang, *et al.*, Comparison of chromium poisoning between lanthanum strontium manganite and lanthanum strontium ferrite composite cathodes in solid oxide fuel cells, *J. Power Sources*, 2020, **476**, 228743.
12 A. Beez, X. Yin, N. H. Menzler, R. Spatschek and M. Bram, Insight into the Reaction Mechanism of $(La_{0.58}Sr_{0.40})(Co_{0.20}Fe_{0.80})O_{3-\delta}$ Cathode with Volatile Chromium Species at High Current Density in a Solid Oxide Fuel Cell Stack, *J. Electrochem. Soc.*, 2017, **164**, F3028–F3034.
13 A. Beez, K. Schiemann, N. H. Menzler and M. Bram, Accelerated Testing of Chromium Poisoning of Sr-Containing Mixed Conducting Solid Oxide Cell Air Electrodes, *Front. Energy Res.*, 2018, **6**.
14 M. B. Liu and B. Yildiz, Onset Reaction Mechanism of Cr and S Poisoning on Perovskite Oxide Surfaces, *Chem. Mater.*, 2024, **36**(21), 10571–10582.
15 Y. L. Huang, A. M. Hussain, C. Pellegrinelli, C. Xiong and E. D. Wachsman, Chromium Poisoning Effects on Surface Exchange Kinetics of $La_{0.6}Sr_{0.4}Co_{0.2}Fe_{0.8}O_{3-\delta}$, *ACS Appl. Mater. Interfaces*, 2017, **9**, 16660–16668.
16 S.-N. Lee, A. Atkinson and J. A. Kilner, Effect of Chromium on $La_{0.6}Sr_{0.4}Co_{0.2}Fe_{0.8}O_{3-\delta}$ Solid Oxide Fuel Cell Cathodes, *J. Electrochem. Soc.*, 2013, **160**, F629–F635.
17 E. Bucher, M. Yang and W. Sitte, *In Situ* Investigations of the Chromium-Induced Degradation of the Oxygen Surface Exchange Kinetics of IT-SOFC Cathode Materials $La_{0.6}Sr_{0.4}CoO_{3-\delta}$ and $La_{0.58}Sr_{0.4}Co_{0.2}Fe_{0.8}O_{3-\delta}$, *J. Electrochem. Soc.*, 2012, **159**, B592–B596.
18 Q. Fang, C. E. Frey, N. H. Menzler and L. Blum, Electrochemical Performance and Preliminary Post-Mortem Analysis of a Solid Oxide Cell Stack with 20000 h of Operation, *J. Electrochem. Soc.*, 2018, **165**, F38–F45.
19 Q. Fang, N. H. Menzler and L. Blum, Degradation Analysis of Long-Term Solid Oxide Fuel Cell Stacks with Respect to Chromium Poisoning in $La_{0.58}Sr_{0.4}Co_{0.2}Fe_{0.8}O_{3-\delta}$ and $La_{0.6}Sr_{0.4}CoO_{3-\delta}$ Cathodes, *J. Electrochem. Soc.*, 2021, **168**, 104505.
20 E. Povoden-Karadeniz, M. Chen, T. Ivas, A. N. Grundy and L. J. Gauckler, Thermodynamic modeling of La_2O_3-SrO-Mn_2O_3-Cr_2O_3 for solid oxide fuel cell applications, *J. Mater. Res.*, 2012, **27**, 1915–1926.
21 H. Yokokawa, *et al.*, Thermodynamic considerations on Cr poisoning in SOFC cathodes, *Solid State Ionics*, 2006, **177**, 3193–3198.
22 X. Yin, L. Bencze, V. Motalov, R. Spatschek and L. Singheiser, Thermodynamic perspective of Sr-related degradation issues in SOFCs, *Int. J. Appl. Ceram. Technol.*, 2018, **15**, 380–390.
23 H. Yokokawa, *et al.*, Thermodynamic and kinetic considerations on degradations in solid oxide fuel cell cathodes, *J. Alloys Compd.*, 2008, **452**, 41–47.
24 X. Chen, L. Zhang and S. P. Jiang, Chromium Deposition and Poisoning on $(La_{0.6}Sr_{0.4-x}Ba_x)(Co_{0.2}Fe_{0.8})O_3$ $(0 \leq x \leq 0.4)$ Cathodes of Solid Oxide Fuel Cells, *J. Electrochem. Soc.*, 2008, **155**, B1093.
25 R. Kiebach, *et al.*, Stability of $La_{0.6}Sr_{0.4}Co_{0.2}Fe_{0.8}O_3$/$Ce_{0.9}Gd_{0.1}O_2$ cathodes during sintering and solid oxide fuel cell operation, *J. Power Sources*, 2015, **283**, 151–161.
26 B. Talic, K. Norrman, T. Sand, J. Froitzheim and P. V. Hendriksen, Correlating Oxygen Electrode Degradation to Cr Vaporization from Metallic Interconnects in Solid Oxide Cell Stacks, *J. Electrochem. Soc.*, 2023, **170**, 124517.
27 M. Kornely, *et al.*, Degradation of anode supported cell (ASC) performance by Cr-poisoning, *J. Power Sources*, 2011, **196**, 7203–7208.
28 N. Ni, C. C. Wang, S. P. Jiang and S. J. Skinner, Synergistic effects of temperature and polarization on Cr poisoning of $La_{0.6}Sr_{0.4}Co_{0.2}Fe_{0.8}O_{3-\delta}$ solid oxide fuel cell cathodes, *J. Mater. Chem. A*, 2019, **7**, 9253–9262.
29 N. Ni, *et al.*, Degradation of $(La_{0.6}Sr_{0.4})_{0.95}(Co_{0.2}Fe_{0.8})O_{3-\delta}$ Solid Oxide Fuel Cell Cathodes at the Nanometer Scale and below, *ACS Appl. Mater. Interfaces*, 2016, **8**, 17360–17370.
30 Q. Fang, L. Blum and D. Stolten, Electrochemical Performance and Degradation Analysis of an SOFC Short Stack Following Operation of More than 100000 Hours, *J. Electrochem. Soc.*, 2019, **166**, F1320–F1325.
31 N. H. Menzler, D. Sebold and O. Guillon, Post-test characterization of a solid oxide fuel cell stack operated for more than 30000 hours: the cell, *J. Power Sources*, 2018, **374**, 69–76.
32 N. H. Menzler, D. Sebold, Y. J. Sohn and S. Zischke, Post-test characterization of a solid oxide fuel cell after more than 10 years of stack testing, *J. Power Sources*, 2020, **478**.

33 C. Dellen, *et al.*, Analysis of Structural Degradation Effects in a Solid Oxide Fuel Cell after Long-Term Operation, *ECS Trans.*, 2023, **111**, 1845–1854.
34 D. Jennings, *et al.*, The Formation of Stacking Faults in Barium Zirconate-Type Perovskites, *Chem. Mater.*, 2023, **35**, 8382–8396.
35 C. Dellen, *et al.*, Analysis of Structural Degradation Effects in a Solid Oxide Fuel Cell after Long-Term Operation, *ECS Meeting Abstracts*, 2023, **MA2023-01**, 287.
36 W. Schafbauer, N. H. Menzler and H. P. Buchkremer, Tape casting of anode supports for solid oxide fuel cells at Forschungszentrum Jülich, *Int. J. Appl. Ceram. Technol.*, 2014, **11**, 125–135.
37 L. G. J. De Haart, J. Mougin, O. Posdziech, J. Kiviaho and N. H. Menzler, Stack degradation in dependence of operation parameters; the real-SOFC sensitivity analysis, *Fuel Cells*, 2009, **9**, 794–804.
38 L. Blum, U. Packbier, I. C. Vinke and L. G. J. De Haart, Long-term testing of SOFC stacks at forschungszentrum jülich, *Fuel Cells*, 2013, **13**, 646–653.